

This item is the archived peer-reviewed author-version of:

Novel two-dimensional ZnO₂, CdO₂ and HgO₂ monolayers: a first-principles-based prediction

Reference:

Faraji M., Bafekry Asadollah, Gogova D., Hoat D.M., Ghergherehchi M., Chuong N.V., Feghhi S.A.H. - Novel two-dimensional ZnO₂, CdO₂ and HgO₂ monolayers: a first-principles-based prediction
New journal of chemistry - ISSN 1144-0546 - Cambridge, Royal soc chemistry, 45(2021), p. 9368-9374
Full text (Publisher's DOI): <https://doi.org/10.1039/D1NJ01610E>
To cite this reference: <https://hdl.handle.net/10067/1782450151162165141>

Cite this: DOI: 10.1039/xxxxxxxxxx

Novel two-dimensional ZnO₂, CdO₂ and HgO₂ monolayers: a first-principles-based prediction

M. Faraji¹, A. Bafekry^{2,3†}, D. Gogova⁴, D. M. Hoat^{5,6}, M. Ghergherehchi⁷, Chuong V. Nguyen⁸, S.A.H Feghhi¹

Received Date

Accepted Date

DOI: 10.1039/xxxxxxxxxx

www.rsc.org/journalname

In this paper, the existence of monolayers with the chemical formula XO₂, where X= Zn, Cd, and Hg with hexagonal and tetragonal lattice structures is theoretically predicted by means of first principles calculations. Through cohesive energy calculation and phonon dispersion simulation, it has been proven that the two-dimensional XO₂ monolayers proposed are energetically and dynamically stable suggesting their potential experimental realization. Our detailed study demonstrates that these novel newly predicted materials are half-metals and dilute magnetic semiconductors as well as they exhibit magnetism in the ground state. The half-metallic character could find many applications in electronic and spintronic devices. Research into the magnetic properties revealed here can enrich theoretical knowledge in this area and provide more potential candidates for XO₂ 2D-based materials and Van der Waals heterostructures.

1 Introduction

The discovery of the first atomically thin two-dimensional (2D) material Graphene¹ with magnificent properties, which have never been observed before, has triggered tremendous pure scientific and technological interest. A huge number of researchers has devoted enormous efforts in exploration of the monolayer carbon and in development of novel 2D materials beyond Graphene such as MXenes,^{2–6} honeycomb-like Xenes (X= Pb, Sn, Ge, and Si)^{6,7}, perovskites⁸, and so on. The 2D materials family has potential applications in nanoscale electronic and optoelectronic devices⁹, and photocatalytic hydrogen productions¹⁰. Among 2D materials, some behave like insulators, others as¹¹, semiconductors¹², metals¹³, semi-metals¹⁴, half-metals^{15,16}, or superconductors¹⁷. II-VI group semiconductors or group II-chalcogenide

materials with the general formula of AX (where A is referred to Zn, Cd, Hg, and X to O, S, Se, Te elements) have brought many advantages, and they can be utilized in different fields including photovoltaics^{18–20}, light-emitting diodes^{21–24}, photocatalytic hydrogen production and photoelectrochemical water splitting^{25–27}, optical gain^{28–32}, CO₂ reduction to CO^{33–37} and so on, due to their unique electronic, optical, mechanical properties, and long-term stability. Experimentally, there have been several synthesis methods have been developed for group-II chalcogenide compounds, including colloidal approach³⁸, colloidal ALD³⁹, chemical bath deposition⁴⁰, CVD⁴¹. Their unique properties have been revealed by a lot of theoretical calculations and analytical methods^{42–47}.

Nanoscaled ZnO, CdO, and HgO oxide compounds, have been a subject of many investigations both experimentally and theoretically (based on DFT calculation^{48–52} due to their exceptional physical and chemical properties. In general, they are wide-bandgap semiconductors with potential applications from the ultraviolet to the deep blue spectral region similar to III-nitrides and Ga₂O₃⁵³. They have a tendency to be inherent n-type semiconductors and p-type doping poses a serious issue in these materials. In addition to aforementioned oxide compounds, the transition metal peroxides such as zinc peroxide (ZnO₂), cadmium peroxide (CdO₂), and mercury peroxide (HgO₂) could be new candidates for 2D structures still unknown properties. It should be noted that bulk trigonal and cubic ZnO₂ structures have been depicted magnetic and non-magnetic properties, respectively. Trigonal ZnO₂ structure has a band gap of about 4 eV with insulating

¹Micro and Nanotechnology Graduate Program, TOBB University of Economics and Technology, Sogutozu Caddesi No 43 Sogutozu, 06560, Ankara, Turkey.

²Department of Radiation Application, Shahid Beheshti University, Tehran 1983969411, Iran. Email: Bafekry.asad@gmail.com

³Department of Physics, University of Antwerp, Groenenborgerlaan 171, B-2020 Antwerp, Belgium

⁴Department of Physics, University of Oslo, P.O. Box 1048, Blindern, Oslo, Norway

⁵Institute of Theoretical and Applied Research, Duy Tan University, Hanoi 100000, Vietnam

⁶Faculty of Natural Sciences, Duy Tan University, Da Nang 550000, Vietnam

⁷College of Electronic and Electrical Engineering, Sungkyunkwan University, Suwon, Korea

⁸Department of Materials Science and Engineering, Le Quy Don Technical University, Hanoi 100000, Vietnam

† To whom correspondence should be addressed.

properties, while cubic ZnO₂ structure depicts a semiconductor with a band gap of 2.157 eV. For the bulk CdO₂, both cubic and monoclinic structures have been depicted non-magnetic properties. Both CdO₂ structures show an indirect semiconductor with a bandgap of 1.268 and 2.36 eV for cubic and monoclinic structures, respectively. Finally, for the bulk HgO₂ with orthorhombic and monoclinic structures, both have been depicted as non-magnetic materials, with an indirect bandgap of 0.308 and 0.212 eV, respectively. The ZnO₂ structure has two oxygen atoms which are linked by a single bond. It has gathered large scientific interest because of the high electronegativity due to the excess of oxygen, especially on a nanoscale level.

Nanostructured ZnO₂ has been successfully utilized in contamination removal from water by UV irradiation⁵⁵ as well as in detoxification of mustard gas⁵⁶. The ZnO₂ powder used in many areas, including cosmetics, wear resistance, oral surgeries, and so on⁵⁶. However, while the photocatalytic properties of different 2D metal oxides structures^{57–60} have been studied until now, the photocatalytic properties of metal peroxides and related composite materials require detailed investigation. A. G. El-Shamy⁶¹ reported on photocatalytic and tunable photoluminescence performance of carbon quantum dots (CQDs) and ZnO₂ nanocomposites. The results have depicted a larger photocatalytic activity of the CQDs/ZnO₂ nanoparticles than pristine TiO₂, and ZnO₂ structures, against Rh.B, Mo, and MB degradation degradation than of the pristine TiO₂, and ZnO₂ structures. CdO₂ is a semiconductor with a bandgap of 2.33 eV. It can be synthesized with different methods^{62–64} and utilized in fields such as photocatalyst⁶⁵, a precursor for CdO n-type semiconductor synthesis⁶⁶, and as an additive material in the rubber and plastic industry⁶⁴. Several theoretical studies (first-principle calculations) have been implemented to understand the CdO₂ structure. For example, A. Zaoui and M. Ferhat,⁶⁷ reported a thermodynamically and mechanically stable a cubic CdO₂ semiconductor structure with bandgap of 2.9 eV. Nanostructured mercury compounds have been used in different applications^{68–71}.

The origin of 1H and 1T phase configuration goes back to MoS₂ different phases, including 1H, 2H, 1T, and so on. Among these phases, two of them are favorable from a structural point of view: 1H-MoS₂ possesses a very rich physics and chemistry. The 1T-MoS₂ structure is a metastable phase, and the most significant distinction between the H and T phase is that 1T-MoS₂ structure depicts metallic properties, while 1H and 2H is an insulator or a semiconductor⁷². By following the phase structural differences modeling and synthesis, scientists started to develop other structural materials in different phases both theoretically and experimentally, such as semimetal 1H-SnS₂⁷³, metallic H-TaS₂⁷⁴, and H-TaSe₂⁷⁵, semiconductor 1T-PtSe₂⁷⁶, semiconductor 1T-HfSe₂⁷⁷, and so on. Obviously, to have different electronic properties of the same materials, it is better to synthesize the material in different phases. XO₂ structures are also following the phase structural differences, which depict different electronic properties behavior. As the same as a 1H-MoS₂ monolayer, our 1H-XO₂ structures can be considered as the pristine structures for other XO₂ related structures.

However, there is no a single study on nanostructured HgO₂ in

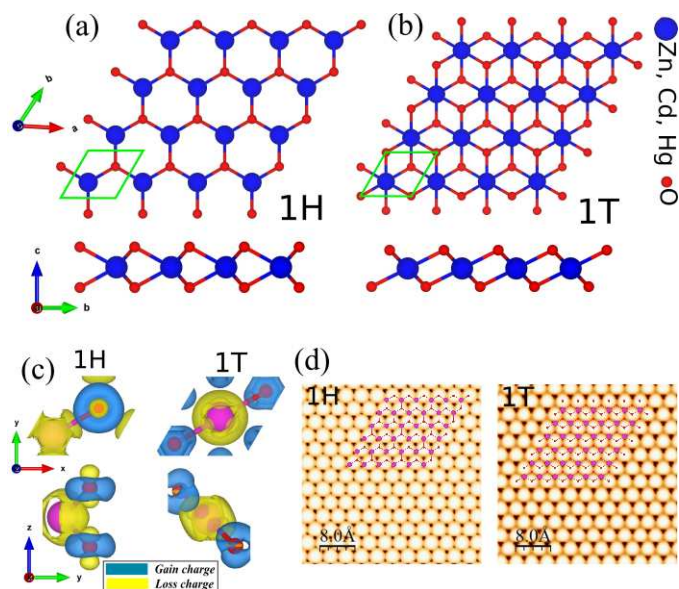


Fig. 1 Atomic structures of XO₂ (X= Zn,Cd,Hg) monolayers (a) -1H and (b) -1T phases, with a primitive unit cell indicated by a green parallelogram. (c) Difference charge density of CdO₂-1H and -1T monolayers. (d) Simulated STM images of CdO₂-1H and -1T monolayers. The inset structure represents repeating the unit cell.

the literature. Theoretically, DFT modeling of HgO₂ can stimulate new research on understanding ructure mercury peroxide compounds. In this paper, the stability as well as structural, electronic and magnetic properties of XO₂ (X= Zn,Cd,Hg) monolayers with hexagonal (1H) and tetragonal (1T) structures have been investigated by means of the first-principle calculations. XO₂ monolayers with 1H and 1T structures are found to be dynamically stable. Our calculation results demonstrate that the XO₂ monolayers are half-metal and exhibit magnetism in the ground state, i.e. they could open a new door in technology and applications.

2 Method

The structural optimization and electronic properties were performed by the plane-wave basis projector augmented wave (PAW) method in the framework of density-functional theory (DFT). The generalized gradient approximation (GGA) with Perdew-Burke-Ernzerhof(PBE)^{77,78} exchange-correlation functional was used for exchange and correlation contributions as implemented in the Vienna *ab-initio* Simulation Package (VASP)^{79,80}. Analysis of the charge transfers in the structures was determined by the Bader technique⁸⁵. The kinetic energy cut-off for plane-wave expansion was set to 500 eV and the energy was minimized until its variation in the following steps became 10⁻⁸ eV. To get the optimized structures, the total Hellmann-Feynman forces were reduced to 10⁻⁷ eV/Å. 21×21×1 Γ centered *k*-point sampling was used or the primitive unit cells by using Monkhorst-Pack⁸⁶. Monolayers have been modeled with vacuum region 20 Å to avoid interaction between neighboring slabs. The vibrational properties were obtained from the small displacement method as implemented in the PHON code⁸⁷. Simulated scanning tunneling microscopy (STM) images were obtained using the Tersoff-Hamann theory⁸³. The STM simulated images were graphically presented using the

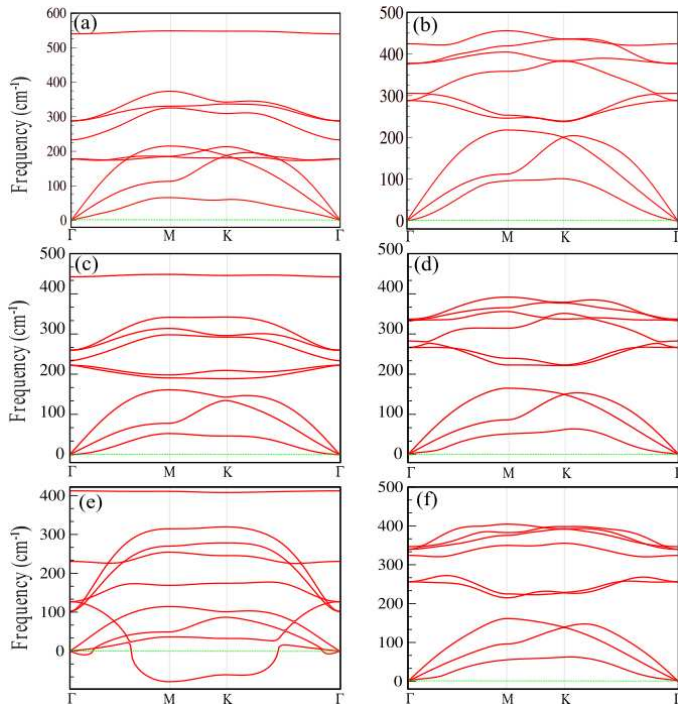


Fig. 2 Phonon band dispersion of (a) ZnO₂-1H, (b) ZnO₂-1T, (c) CdO₂-1H, (d) CdO₂-1T and (e) HgO₂-1H and (f) HgO₂-1T monolayers.

WSxM software⁸⁴. The training set was prepared by conducting ab-initio molecular dynamics (AIMD) simulations over $2 \times 2 \times 1$ supercells with $2 \times 2 \times 1$ k-points. AIMD simulations were carried out at 50 and 600 K, each for 1000 time steps. Half of the AIMD trajectories are selected to create the training sets.

3 Monolayer of XO₂ (X= Zn,Cd,Hg)

3.1 Structural properties

The honeycomb structures of the XO₂ monolayers exhibit space group P_{3m1} , as shown in Figs. 1(a) and (b), respectively. The hexagonal primitive unit cell is formed by four atoms and the vectors $\vec{a} \neq \vec{b}$ are the translational unit cell vectors. Before gaining insight into the electronic properties, we first calculate the geometrical structure, with full optimization of all the atoms and determine the crystal lattice parameters. The calculated lattice constants of the ZnO₂ are equal to 3.08 Å (1H) and 3.11 Å (1T), while the bond lengths d_1 and d_2 are determined to be 2.07 Å (1H) and 2.11 Å (1T), respectively. The two angles of the Zn-O-Zn bonds in the ZnO₂-1H (1T) lattice are 96.21° (79.84°) and 61.47° (100.13°), i.e. slightly deviating from 120° and indicating the in-plane anisotropy of the lattice. In the CdO₂-1H (-1T), we found that the lattice parameters increase to 3.44 (3.40) Å, while the bond lengths are $d_1=2.27$ (2.23) Å and $d_2=2.20$ (2.82) Å. In addition, the bond angles are same $\theta_1=98.44^\circ$ and $\theta_2=58.05^\circ$ for each CdO₂-1H layer as well as the thickness of the CdO₂ is determined to be 2.55 Å. Notice that in the case of HgO₂-1T structure, the lattice parameter is determined to be 3.00 Å. We found out that the bond lengths are 2.24 and 2.89 Å, while the bond angles are calculated 80.21 and 99.80°, respectively. The difference charge density of CdO₂-1H and -1T is depicted in Fig. 1(c),

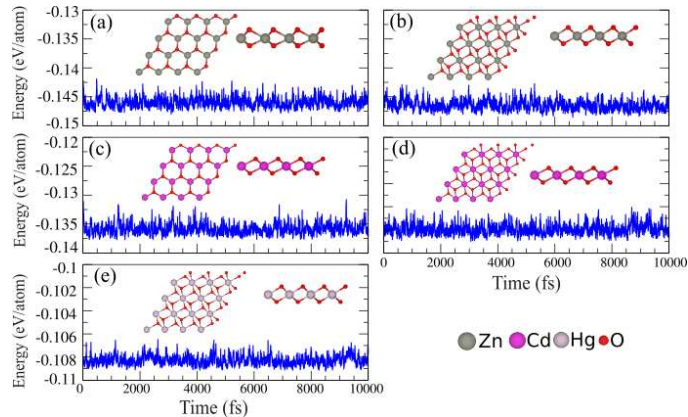


Fig. 3 Ab initio molecular dynamics (AIMD) for the (a) ZnO₂-1H, (b) ZnO₂-1T, (c) CdO₂-1H, (d) CdO₂-1T and (e) HgO₂-1T monolayers at room temperature. The top and side views of the structures after 5 ps of simulation indicated as inset.

where the blue and yellow regions represent the charge accumulation and depletion, correspondingly. The difference charge density ($\Delta\rho$) is defined as follows:

$$\Delta\rho = \rho_{XO_2} - \rho_X - \rho_O \quad (1)$$

where ρ_{XO_2} , ρ_X and ρ_O represents the charge densities of the XO₂ and isolated atoms, respectively. From the difference charge density, we found out that the negatively charged O atoms are surrounded by positively charged X atoms. We discover that each O atom gains about 1.33 e , and 1.27 e from the adjacent Zn and Cd atoms in ZnO₂-1H and CdO₂-1H structures, respectively. Meanwhile, in the 1T structure of ZnO₂, CdO₂ and HgO₂, each O atom gains about 1.40, 1.32 and 1.22 e from the adjacent Zn, Cd and Hg atoms. The charge redistribution is due to the different electro-negativity of Zn (1.65), Cd (1.69), Hg (2.00) and O (3.44). Simulated STM image of the CdO₂-1H (left) and -1T (right) is illustrated in Fig. 1(d), which overlaid with its structure. From the theoretically predicted STM images, it is easy to recognize and correlate them with the corresponding atomistic structure. One can see the the O atoms are brighter than the Cd ones. Cohesive energy, which is defined as the energy required to separate condensed material into isolated free atoms, is one of the most important physical parameters for quantifying the energetic stability of materials. The cohesive energy per atom was calculated using the following equation:

$$E_{coh} = \frac{E_{tot} - E_X - 2E_O}{n_{tot}} \quad (2)$$

where E_X and E_{Bi} represent the energies of isolated single X (Zn, Cd and Hg) and O atoms, n_{tot} is the total number of unit cell, respectively; E_{tot} represents the total energy of the XO₂ monolayer. The cohesive energy of ZnO₂-1H and -1T, are found to be -2.88 and -3.00 eV/atom, respectively, which indicates that the formation of 1T is more favorable than 1H. In addition, the calculated cohesive energy of CdO₂-1H (-2.55 eV/atom) and CdO₂-1T (-2.62 eV/atom) indicates the magnetic ground state of the 1T is more favorable. Notice, the cohesive energy of HgO₂-1T is

Table 1 The structural, electronic and magnetic parameters of XO_2 -1H and -1T monolayers. The corresponding structural, electronic and magnetic parameters including lattice constant a ; the bond lengths between X-O atoms $d_{1,2}$; the bond angles between X-O atoms $\theta_{1,2}$; the thickness layer (t); the cohesive energy per atom, (E_{coh}); the charge transfer (ΔQ) between atoms; the magnetic moment per unitcell M_{tot} ; Electronic states (ES) are specified as half-metal (HM) and Dilute magnetic semiconductor (DMS). The band gap (E_g) of PBE functional in the up-spin channel.

	a (Å)	d_1 (Å)	d_2 (Å)	t (Å)	$\theta_{1,2}$ (°)	E_{coh} (Å)	ΔQ (eV/atom)	Φ (e)	ES (eV)	M_{tot} (μ_B)	E_g (eV)
ZnO ₂ -1H	3.08	2.07	2.11	2.57	96.21,61.47	2.88	1.33	7.72	HM	2	0
ZnO ₂ -1T	3.11	2.03	2.60	2.57	79.84,100.13	3.00	1.40	7.46	DMS	2	0.25
CdO ₂ -1H	3.44	2.27	2.20	2.57	98.44,58.05	2.55	1.27	7.26	HM	2	0
CdO ₂ -1T	3.40	2.23	2.82	2.57	100.138,78.67	2.62	1.32	7.24	DMS	2	0.05
HgO ₂ -1T	3.00	2.24	2.89	2.57	80.21,99.80	2.03	1.22	7.21	DMS	2	0.21

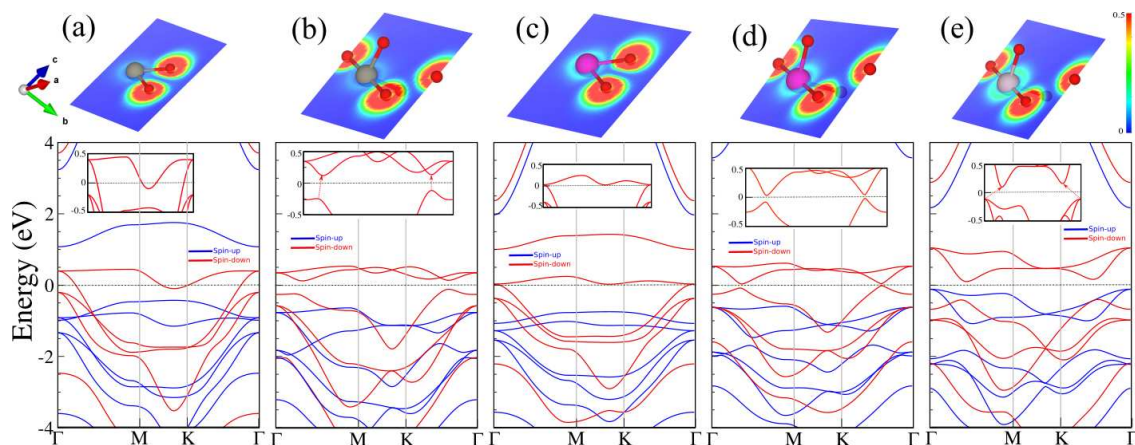


Fig. 4 Electronic band structure of (a) ZnO₂-1H, (b) ZnO₂-1T, (c) CdO₂-1H, (d) CdO₂-1T and (e) HgO₂-1T. Contour plot of the electron localization function (ELF), are shown in the top of panels. Red (blue) color indicate high (low) electron density. The zero of energy is set to Fermi-level.

obtained -2.03 eV/atom. The more negative values for cohesive energies suggest that the energetically more stable monolayer, and the structures represent more stability when the atoms get lighter. Now we examine the dynamical and thermal stability of XO_2 monolayer by evaluating the phonon dispersion relation and AIMD trajectories at 500 K, respectively. The dynamical stability is verified by calculating the phonon band dispersions, as presented in in Figs. 2(a-f). Apparently, phonon branches are free from any imaginary frequencies indicating the dynamical stability of all the XO_2 monolayers, except HgO₂-1H, as depicted in Fig. 2(e). It demonstrates the instability of the HgO₂-1H monolayer. Ab initio molecular dynamics (AIMD) and for the studied monolayers at room temperature is shown in Figs. 3(a-e). The top and side views of the structures after 5 ps of simulation as insets is shown in Fig. 3. Analysis of the AIMD trajectories also shows that the structure could stay intact at 300 K, with very stable energy and temperature profiles, proving the thermal stability of the XO_2 monolayer.

3.2 Electronic and magnetic properties

The electronic band structure of the XO_2 monolayers are depicted in Figs. 4(a-e). The contour plot of the electron localization function (ELF), are shown in the top of panels, which red and blue colored indicate high and low electron density, respectively. Notice, that ZnO₂-1H exhibit a half-metallic behavior with valence bands in the \downarrow spin channel, crossing the Fermi level and has $2 \mu_B$

magnetic moment. While ZnO₂-1T, shows semiconducting characteristics in both of \uparrow and \downarrow spin channels, i.e., it is a dilute. The direct band gap of ZnO₂-1T in the \downarrow spin channels is calculated to be 0.21 eV, while the valance band minimum (VBM) and conduction band maximum (CBM) are located along the K- Γ points. Notice that, we can see a direct band gap with a value of 0.27 meV, which is located along the Γ -M points. The magnetic moment of the ZnO₂-1T is determined to be $2 \mu_B$ in the ground state. Similarly ZnO₂, CdO₂ exhibit HM and DMS in the 1H and 1T phases structures and our results show that the magnetic moment of the CdO₂-1T and -1H is $2 \mu_B$ in the ground state. In the \downarrow spin channels of the CdO₂-1T, we can see a narrow direct band gap of 50 meV, while the VBM and CBM are located between the K and Γ points. Pay attention, we found a narrow direct band gap with a value of 110 meV, which are located between the Γ and M points. In the case of HgO₂-1T, the \uparrow and \downarrow spin channels are splitted, result in show a DMS and induce $2 \mu_B$ magnetic moment in the ground state. The indirect band gap of the HgO₂-1T in the \downarrow spin channels is calculated to be 0.25 eV, while the VBM and CBM is located along the Γ -M points. Notice that, a direct band gap of 0.35 eV, is shown in the along K- Γ points.

Since these monolayers are semiconductor in the \uparrow and \downarrow spin channels, the HSE06 functional was also used to study the electronic band structures, shown in Fig. S2. Based on the acquired band structure by HSE06 method, the ZnO₂-1H and ZnO₂-1T monolayers exhibits a half-metallic characteristic. Our results

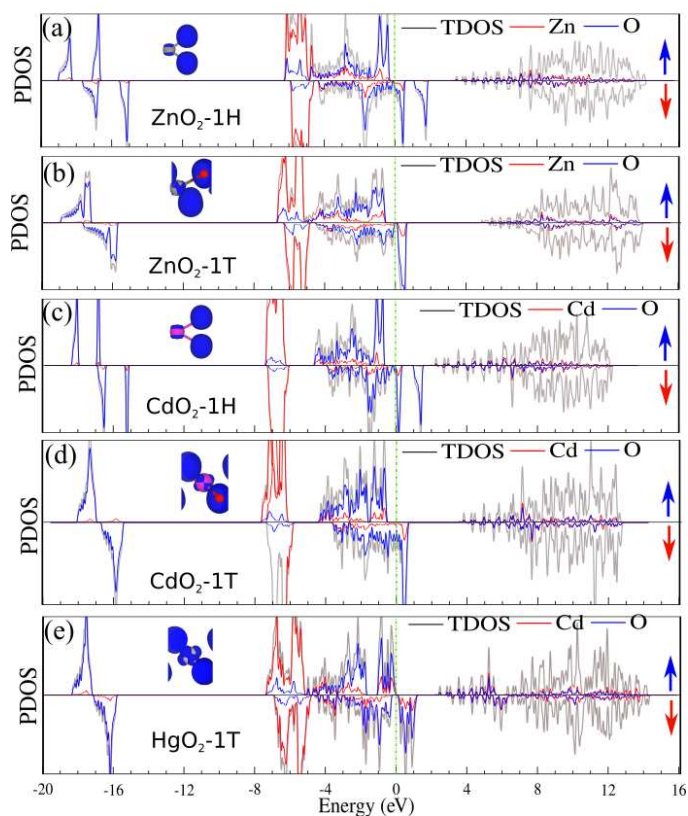


Fig. 5 DOS and PDOS of (a) ZnO_2 -1H, (b) ZnO_2 -1T, (c) CdO_2 -1H, (d) CdO_2 -1T and (e) HgO_2 -1T. Difference spin density are shown in the insets. The blue and yellow regions represent the \uparrow and \downarrow spin states, respectively. The zero of energy is set to Fermi-level.

shows that CdO_2 shows DMS and half-metallic behaviors in the 1H and 1T phases structures, respectively. In the case of HgO_2 -1T, the \uparrow (\downarrow) spin channels is semiconductor (metal), result in shows a half-metallic in the ground state.

In order to explain the origin of the electronic states, the density of states (DOS) and projected DOS (PDOS) is shown in Fig. 5. The contribution of different atomic orbitals indicated in Fig. S1 in the supplementary information (SI). Evidently, that the metallic character of the ZnO_2 -1H and CdO_2 -H comes from the O atoms in the \downarrow spin channel, while Zn and Cd atoms do not show any contribution (see Fig. 5). From DOS and PDOS of the ZnO_2 -1T and CdO_2 -T, we can see that the VBM originates from the O- $p_{x,y}$ orbitals (\uparrow spin channels), while the CBM consists of O- p_z orbital states (\downarrow spin channels). Unlike the ZnO_2 -1T, we found that the VBM and CBM of HgO_2 -1T originates from the O- p_z (\uparrow spin channel) The difference spin density is calculated from the difference spin density between \uparrow and \downarrow spin channels. In order to analyses the magnetism, the difference spin density of the XO_2 , is illustrated in the inset of Fig. 5. One can conclude that the magnetism mainly originates from the O atoms in XO_2 .

Due to the weak screening of the Coulomb interaction in 2DM, it is expected that the Hubbard U will be larger than in three-

dimensional materials, thus the energy band gap may be expected to be enhanced significantly. We investigate effects of correlation by varying the value of the Hubbard U, since the accurate value of U has not been determined for ZnO_2 -1H and CdO_2 -H monolayers. The electronic band structure of ZnO_2 -1H and CdO_2 -H monolayers as a function of Hubbard U, is shown in Figs. S3(a,b). We see from the Fig. S3(a) that the ZnO_2 -1H still maintains the DHM feature even when considering the effect of the Hubbard U. With increase of Hubbard U, the 3d orbitals of Zn atom states do not change near Fermi-level, indicating the robustness of energy bands against the correlation effect in Zn-3d electrons. The correlation effects on the electronic properties of CdO_2 -H significant and we can see that the CdO_2 -H still maintains the DMS character. Notice, the band gap increasing in the \downarrow spin channel is a result of a cooperative effect of electron correlation for the CdO_2 -H. Our results show that the band gap (\downarrow spin channel) of CdO_2 -H increases from 1.25 eV for $U = 1$ eV to 2 eV for $U = 8$ eV, and therefore DMS remains for $U = 1$ -8 eV.

4 Conclusion

In summary, we have investigated the structural, dynamical stability, thermal stability, electronic and magnetic properties of novel 2D materials- XO_2 ($X = \text{Zn, Cd, Hg}$) - by using first-principles calculations. Our computational results have proven the energetic and dynamic stability of this new class of 2D materials with amazing properties. Thus, our study could trigger the search for methods of synthesis of ZnO_2 , CdO_2 and HgO_2 monolayers and exploration of their high application potential. Research into the magnetic properties revealed here can enrich theoretical knowledge in this area and provide more potential candidates for XO_2 2D-based materials and Van der Waals heterostructures.

ACKNOWLEDGMENTS

This work was supported by the National Research Foundation of Korea (NRF) grant funded by the Korea government (MSIT) (NRF-2015M2B2A4033123).

DATA AVAILABILITY

The data that support the findings of this study are available from the corresponding author upon request

References

- 1 K. S. Novoselov, A. K. Geim, S. V. Morozov, D. Jiang, Y. Zhang, S. V. Dubonos, I. V. Grigorieva, A. A. Firsov, *Sci.* 306, 5696, (2004) 666-669.
- 2 A. Bafekry, B. Akgenc, M. Ghergherehchi, and F. M. Peeters, *J. Phys. Condens. Matter.* (2020) 29, 355504.
- 3 A. Bafekry, C.V. Nguyen, C. Stampfl, B. Akgenc and M. Ghergherehchi, *Phys. Status Solidi B*, (2020).
- 4 E. M. D. Siriwardane, I. Demiroglu, C. Sevik, F. M. Peeters, and D. Cakir, *J. Phys. Chem. C* (2020), 124, 39, 21293-21304.
- 5 Q. Zhao, M. Seredych, E. Precetti, C. E. Shuck, M. Harhay, R. Pang, C. Shan, and Y. Gogotsi, *ACS Nano*, 14, 9, (2020), 11787-11798.

- 6 A. Bafekry, F. Shojaei, M. M. Obeid, M. Ghergherehchi, C. Nguyen, and M. Oskouian, *RSC Adv.*, (2020), 10, 31894.
- 7 A. Bafekry, F. Shojai, D. M. Hoat, M. Ghergherehchi, C. Nguyen and M. Shahrokhi,
- 8 Y. Chen, Y. Sun, J. Peng, J. Tang, K. Zheng, and Ziqi Liang, *Adv. Mater.* (2017), 1703487.
- 9 S. Kang, D. Lee, J. Kim, A. Capasso, C. H. Lee and G. H. Lee, H. S. Kang, J. W. Park, *2D Mater.*, 7, 2, (2020), 022003.
- 10 Q. Su, Y. Li, R. Hu, F. Song, S. Liu, C. Guo, S. Zhu, W. Liu, and Jian Pan, *Adv. Sustainable Syst.* (2020), 2000130.
- 11 J. Yin, J. Li, Y. Hang, J. Yu, G. Tai, X. Li, Z. Zhang, and W. Guo, *small*, 12, 22, (2016), 2942-2968.
- 12 M. Khosravi, G. Moafpouriana, H. A. Badehianb, *Optik*, 218, (2020), 165247.
- 13 D. Zhou, Q. Meng, N. Si, X. Zhou, S. Zhai, Q. Tang, Q. Ji, M. Zhou, T. Niu, and H. Fuchs, *ACS Nano*, 14, (2020), 2385-2394.
- 14 H. Yang, M. Schmidt, V. Suss, M. Chan, F. F. Balakirev, R. D. McDonald, S. S. P. Parkin, C. Felser, B. Yan and P. J. W. Moll, *New J. Phys.* 20, (2018), 043008.
- 15 A. Bafekry, B. Mortazavic, S. Farjami Shayesteha, *J. Magnet. Magnet. Mater.*, 491, (2019), 165565.
- 16 A. Bafekry, C. Stampfl, M. P. Francois, *Sci. Rep.* 10, (2020), 213.
- 17 V. Kamysbayev, Al. S. Filatov, H. Hu, X. Rui, F. Lagunas, D. Wang, R. F. Klie, D. V. Talapin, *Science* 369, 6506, (2020), 979-983.
- 18 R. W. Crisp, F. S. M. Hashemi, J. Alkemade, N. Kirkwood, G. Grimaldi, S. Kinge, L. D. A. Siebbeles, J. R. V. Ommen, and A. J. Houtepen, *Adv. Mater. Interfaces* (2020), 1901600.
- 19 D. B. Li, S. S. Bista, Z. Song, R. A. Awni, K. K. Subedi, N. Shrestha, P. Pradhan, L. Chen, E. Bastola, C. R. Grice, A. B. Phillips, M. J. Heben, R. J. Ellingson, Y. Yan, *Nano Energy*, 73, (2020), 104835.
- 20 P. Labouchere, A. K. Chandiran, T. Moehl, H. Harms, S. Chavhan, R. Tena-Zaera, M. K. Nazeeruddin, M. Graetzel, and N. Tetreault, *Adv. Energy Mater.* (2014), 1400217.
- 21 J. Lim, Y. S. Park, K. Wu, H. J. Yun, and V. I. Klimov, *Nano Lett.* 18, 10, (2018), 6645-6653.
- 22 J. Lim, B. G. Jeong, M. Park, J. K. Kim, J. M. Pietryga, Y. S. Park, V. I. Klimov, C. Lee, D. C. Lee, and W. Ki Bae, *Adv. Mater.* (2014), 26, 8034-8040.
- 23 J. Roh, Y. S. Park, J. Lim and V. I. Klimov, *Nat Commun* 11, 271 (2020).
- 24 Y. Altintas, B. Liu, P. L. Hernandez-Martinez, N. Gheshlaghi, F. Shabani, M. Sharma, L. Wang, H. Sun, E. Mutlugun, and H. V. Demir, *Chem. Mater.* 32, 18, (2020), 7874-7883.
- 25 C. T. Altaf, M. Faraji, A. Kumtepe, N. Abdullayeva, N. Yilmaz, E. Karagoz, A. Bozbey, H. Kurt, M. Sankir, N. D. Sankir, *J. All. Compound.*, 828, (2020) 154472.
- 26 M. M. Obeid, C. Stampfl, A. Bafekry, Z. Guane, H. R. Jappor, C. V. Nguyen, M. Naseri, D. M. Hoat, N. N. Hieu, A. E. Krauklis, T. V. Vu and D. Gogova, *Phys. Chem. Chem. Phys.*, 22, (2020), 15354-15364.
- 27 M. M. Obeida, A. Bafekry, S. U, Rehmand, C. V. Nguyenf, *Appl. Surf. Sci.*, 534, (2020) 147607.
- 28 O. Erdem, S. Foroutan, N. Gheshlaghi, B. Guzelurk, Y. Altintas, and H. V. Demir, *Nano Lett.* 20, 9, (2020), 6459-6465.
- 29 B. T. Diroll, D. V. Talapin and R. D. Schaller, *ACS Photonics* 4, 3, (2017), 576-583.
- 30 V. Pinchetti, F. Meinardi, A. Camellini, G. Sirigu, S. Christodoulou, W. K. Bae, F. D. Donato, L. Manna, M. Zavelani-Rossi, I. Moreels, V. I. Klimov and S. Brovelli, *Effect of Core/Shell Interface on Carrier Dynamics and Optical Gain Properties of Dual-Color Emitting CdSe/CdS Nanocrystals*, *ACS Nano* 10, 7, (2016), 6877-6887.
- 31 J. Lim, Y. S. Park and V. I. Klimov, *Optical gain in colloidal quantum dots achieved with direct-current electrical pumping*, *Nat. Mater.* 17, (2018), 42-49.
- 32 K. Wu, Y. S. Park, J. Lim and V. I. Klimov, *Nat. Mater.* 17, (2018), 42-49.
- 33 F. Zhang, Y. H. Li, M. Y. Qi, Z. R. Tang, and Y. J. Xu, *Applied Catalysis B: Environmental*, 268, (2020), 118380.
- 34 D. Tan, W. Lee, Y. E. Kim, Y. N. Ko, Y. E. Jeon, J. Hong, S. K. Jeong and K. T. Park, *ACS Sustainable Chem. Eng.* 8, 29, (2020), 10639-10645.
- 35 N. Q. Thang, A. Sabbah, L. C. Chen, K. H. Chen, L. V. H. C. M. Thi, P. V. Viet, *Chemical Engineering Science*, 229, (2021), 116049.
- 36 F. Y. Gao, R. C. Bao, M. R. Gao and S. H. Yu, *J. Mater. Chem. A*, 8, (2020), 15458-15478.
- 37 P. Prabhu, V. Jose and J. M. Lee, *Adv. Funct. Mater.* (2020), 1910768.
- 38 M. J. Grotevent, C. U. Hail, S. Yakunin, D. Bachmann, M. Calame, D. Poulidakos, M. V. Kovalenko, I. Shorubalko, *ChemRxiv Preprint*.
- 39 L. Piveteau, D. N. Dirin, C. P. Gordon, B. J. Walder, T. C. Ong, L. Emsley, C. Coperet and M. V. Kovalenko, *Nano Lett.* 20, 5, (2020), 3003-3018.
- 40 R. Vignesh, B. A. kumar, A. Muthuvinayagam, T. Elangovan, K. Kaviyarasu, G. Theophil Anand, G. Ramalingam, *Materials Today: Proceedings*, (2020), 2214-7853.
- 41 J. Luo, Z. Zheng, S. Yan, M. Morgan, X. Zu, X. Xiang and W. Zhou, *ACS Photonics*, 7, 6, (2020), 1461-1467.
- 42 N. Gheshlaghi, M. Faraji, H. Sedaghat Pisheh, *Structural dependent, dielectric and conduction analysis of CdSe based quantum dots*, *Appl. Sci.*, (2019), 401.
- 43 N. Gheshlaghi, M. Faraji, H. Sedaghat Pisheh, *SN Appl. Sci.* 2, (2020), 745.
- 44 N. Gheshlaghi, H. Sedaghat Pisheh, H. Unlu, *Superlattices and Microstructures*, 111, (2017), 156-165.
- 45 N. Gheshlaghi, H. Sedaghat Pisheh, M. R. Karim, H. Unlu, *Energy Procedia*, 102, (2016) 152-163.
- 46 N. Gheshlaghi, H. Sedaghat Pisheh, M. R. Karim, D. Malkoc, H. Unlu, *Superlattices and Microstructures*, 111, (2016), 486-494.
- 47 H. Sedaghat Pisheh, N. Gheshlaghi, H. Unlu, *Physica E*, 85, (2017), 334-339.

- 48 R. Chandiramouli, B. G. Jeyaprakash, *Solid State Sciences*, 16, (2013) 102-110.
- 49 A. Schleife, F. Fuchs, J. Furthmuller, and F. Bechstedt, *PHYSICAL REVIEW B*, 73, (2006), 245212.
- 50 S. Vyas, *Johnson Matthey Technology Review*, 64,2, (2020), 202-218.
- 51 K. Harun, N. A. Salleh, B. Deghfel, M. K. Yaakob and A. A. Mohamad, *Results in Physics*, 16, (2020), 102829.
- 52 P. A. Glans, T. Learmonth, K. E. Smith, J. Guo, A. Walsh, G. W. Watson, F. Terzi, R. G. Egdell, *Physical Review B*, 71, 23, (2005), 235109.
- 53 D. Gogova, A. Kasic, H. Larsson, B. Pecz, R. Yakimova, B. Magnusson, B. Monemar, F. Tuomisto, K. Saarinen, C. Miskys, M. Stutzmann, C. Bundesmann, and M. Schubert, *J. Appl. Phys.* 43 (4A) (2004) 1264-1268.
- 54 D.A. Zatsepin, D.W. Boukhvalov, A.F. Zatsepin, Yu. A. Kuznetsova, D. Gogova, V.Ya. Shur, and A.A. Esin, *Superlattices Microstruct.* 120 (2018) 90-100.
- 55 D. Yanga, M. A. Gondalb, Z. H. Yamanib, U. Baigb, X. Qiaoc, G. Liua, Q. Xud, D. Xiange, J. Maof, K. Shena, *Materials Science in Semiconductor Processing*, 57, (2017), 124-131.
- 56 D. A. Giannakoudakis, M. Florent, R. Wallace, J. Secor, C. Pkarwacki, T. J. Badosz, *Appl. Catal. B: Environ.*, 226, (2018), 429-440.
- 57 R. Saravanan, M. Mansoob Khan, V. K. Gupta, E. Mosquera, F. Gracia, V. Narayanan, g A. Stephen, *J. Coll. Inter. Sci.*, 425, 15, (2015) 126-133.
- 58 R. Saravanan, H. Shankar, T. Prakash, V. Narayanan, A. Stephen, *Mater. Chem. Phys.*, 125, (2011), 277-280.
- 59 T. Munawar, S. Yasmeen, Fayyaz Hussain, K. Mahmood, A. Hussain, M. Asghar, F. Iqbal, *Mater. Chem. Phys.*, 249, (2020), 122983.
- 60 E. A. Abdelrahman, R. M. Hegazey, "Facile Synthesis of HgO Nanoparticles Using Hydrothermal Method for Efficient Photocatalytic Degradation of Crystal Violet Dye Under UV and Sunlight Irradiation, *J. Inorganic and Organometallic Polymers and Materials*, (2019), 29, 346-358.
- 61 A. g. El-Shamy, *Synt. Metal.*, 267, (2020), 116472.
- 62 X. Han, R. Liu, Z. Xu, W. Chen, Y. Zheng, *Electrochemistry Communications*, 7, (2005), 1195-1198.
- 63 L. Beigi, V. Saheb, *Nano-Structures and Nano-Objects*, 9, (2017) 13-18.
- 64 Y. Liu, Y. C. Zhang, M. Zhang, *Mater. Lett.*, 64, (2010) 1779-1781.
- 65 Y. Liu, Y. C. Zhang, X. F. Xu, *J. Hazar. Mater.*, 163, (2009), 1310-1314.
- 66 Y. C. Zhang, G. L. Wang, "Solvothermal synthesis of CdO hollow nanostructures from CdO₂ nanoparticles, *Mater. Lett.*, 62, (2008), 673 - 675.
- 67 A. Zaoui, M. Ferhat, *Phys. Lett. A*, 381, 7, (2017), 685-688.
- 68 N. Goubet, M. Thomas, C. Greboval, A. Chu, J. Qu, P. Rastogi, S. S. Chee, M. Goyal, Y. Zhang, X. Z. Xu, G. Cabailh, S. Ithurria and E. Lhuillier, *J. Phys. Chem. C* 2020, 124, 8423-8430.
- 69 A. Bafekry, M. M. Obeid, C. V. Nguyen, M. Ghergherehchi, M. Bagheri Tagani, *J. Mater. Chem. A*, (2020), 8, 13248-13260.
- 70 M. H. Hudson, M. Chen, V. Kamysbayev, E. M. Janke, X. Lan, G. Allan, C. Delerue, B. Lee, P. G. Sionnest and D. V. Talapin, *ACS Nano* 12, (2018), 9397-9404.
- 71 M. Chen, X. Lan, X. Tang, Y. Wang, M. H. Hudson, D. V. Talapin and P. Guyot-Sionnest, *ACS Photonics* 6, (2019), 2358-2365.
- 72 H. Eidsvag, M. Rasukkannu, D. Velauthapillai, P. Vajeeston, *RSC Adv.*, 11, (2021) 3759-3769.
- 73 Xu, J., Lai, S., Hu, M., Ge, S., Xie, R., Li, F., Hua, D., Xu, H., Zhou, H., Wu, R., Fu, J., Qiu, Y., He, J., Li, C., Liu, H., Liu, Y., Sun, J., Liu, X., Luo, J., *Small Methods*, 4, (2020) 2000567.
- 74 Leyla Najafi, Sebastiano Bellani, Reinier Oropesa-Nuñez, Beatriz Martín-García, Mirko Prato, Lea Pasquale, Jayakumar Panda, Petr Marvan, Zdeněk Sofer, and Francesco Bonaccorso, *ACS Catalysis*, 10, (2020) 3313-3325.
- 75 Junfeng Gao, Yuan Cheng, Tian Tian, Xiaoling Hu, Kaiyang Zeng, Gang Zhang, and Yong-Wei Zhang, *ACS Omega*, 2 (2017) 8640-8648.
- 76 Cai Cheng, Jia-Tao Sun, Xiang-Rong Chen, Sheng Meng, *Science Bulletin* 63, (2018) 85-91.
- 77 J. P. Perdew, K. Burke, and M. Ernzerhof, Generalized gradient approximation made simple, *Phys. Rev. Lett.* 77, 3865 (1996).
- 78 J. P. Perdew, K. Burke, and M. Ernzerhof, Generalized gradient approximation made simple, *Phys. Rev. Lett.* 78, 1396 (1997).
- 79 G. Kresse and J. Hafner, Ab initio molecular dynamics for liquid metals, *Phys. Rev. B* 47, 558 (1993).
- 80 G. Kresse and J. Hafner, Efficient iterative schemes for ab initio total-energy calculations using a plane-wave basis set, *Phys. Rev. B* 49, 14251 (1994).
- 81 J. Heyd, G. E. Scuseria, and M. Ernzerhof, Screened hybrid density functionals applied to solids, *J. Chem. Phys.* 118, 8207 (2003).
- 82 S. J. Grimme, Semiempirical GGA-type density functional constructed with a long-range dispersion correction, *Comput. Chem.* 27, 1787 (2006).
- 83 Tersoff, J. and Hamann, D. R. Theory of the scanning tunneling microscope, *Phys. Rev. Lett.*, 50 (25), 1998-2001, 1983.
- 84 Horcas, I. and Fernandez, R. and Gomez-Rodriguez, J. M. and Colchero, J. and Gomez-Herrero, J. and Baro, A. M. *WSXM: Review of Scientific Instruments*, 78(1):013705, 2007.
- 85 Bader, R. F. W. *Atoms in molecules: a quantum theory* Oxford University Press, (1994) 458 pages: ISBN 978-0-19-855865-1.
- 86 H.J. Monkhorst and J.D. Pack, Special points for Brillouin-zone integrations, *Phys. Rev. B* 13, 12, (1976).
- 87 D. Alfe, PHON: A program to calculate phonons using the small displacement method, *Comput. Phys. Commun.* 180, 2622 (2009).
- 88 M. Gajdos, K. Hummer, G. Kresse, J. Furthmuller, F. Bech-

stedt, Linear optical properties in the projector-augmented wave methodology, *Phys. Rev. B: Condens. Matter Mater. Phys.*, 73 (2006).

- 89 J. Heyd, and G. E. Scuseria, Efficient Hybrid Density Functional Calculations in Solids: Assessment of the Heyd-Scuseria-Ernzerhof Screened Coulomb Hybrid Functional. *J. Chem. Phys.* 2004, 121 (3), 1187-1192.